Available online at www.sciencedirect.com
SCIENCE DIRECT
Journal of Catalysis 241 (2006) 34–44
JOURNAL OF CATALYSIS
www.elsevier.com/locate/jcat

Fe–Zn double-metal cyanide complexes as novel, solid transesterification catalysts

R. Srivastava, D. Srinivas *, P. Ratnasamy *

National Chemical Laboratory, Pune – 411 008, India

Received 25 October 2005; revised 31 March 2006; accepted 1 April 2006

Available online 22 May 2006

Abstract

Fe–Zn double-metal cyanide complexes are currently used as catalysts for the ring-opening polymerization of epoxides, as well as the coupling of epoxides and CO_2 for the production of polycarbonates. We report their novel application as highly efficient solid catalysts for the transesterification reactions of carbonates. The catalysts were prepared from aqueous solutions of $ZnCl_2$ and $K_4Fe(CN)_6$ in the presence of *tert*-butanol (complexing agent) and tri-block copolymer $EO_{20}PO_{70}EO_{20}$ (average molecular weight, 5800; co-complexing agent). They were characterized by chemical analysis, XRD, thermal analysis, N_2 adsorption, magnetic susceptibility, SEM, and FTIR, diffuse reflectance UV–visible, EPR, and X-ray photoelectron spectroscopies. Their acidity was determined from the IR spectra of adsorbed pyridine and the temperature-programmed desorption of NH_3. Catalyst samples prepared with both complexing and co-complexing agents were found to be more acidic and catalytically active than those prepared without these agents. These catalysts are more active/selective than other solid catalysts hitherto reported. Dimethyl carbonate, for example, could be synthesized with 100% selectivity and an isolated yield of >86% by the reaction of propene carbonate with methanol. The catalysts can be recycled without significant loss in activity. Lewis acidic Zn ions are the possible active sites for the transesterification reaction.

Keywords: Double metal cyanide Fe–Zn complexes; Transesterification catalyst; Cyclic carbonate; Organic carbonate; Dimethyl carbonate

1. Introduction

Double-metal cyanide complexes, prepared by the reaction of potassium hexacyanocobaltate(III) and zinc chloride in the presence of complexing agents, are well-known catalysts for the copolymerization of epoxides and CO_2, yielding biodegradable polycarbonates [1–4], and synthesis of propene oxide-based polyether polyols, such as polypropylene glycols (PPG), which are used in a wide range of polyurethane applications [5–11]. These complexes are insoluble in almost all solvents, including aqua-regia. Fe^{3+}–Zn^{2+} complexes are less active than their Co^{3+}–Zn^{2+} analogs [12–14]. Catalysts prepared in the presence of complexing agents are more active than those prepared without these agents. Here we report a novel catalytic application of double-metal cyanide Fe^{2+}–Zn^{2+} complexes as highly efficient solid catalysts for the transesterification of carbonates to dialkyl carbonates.

Dialkyl carbonates, especially dimethyl carbonate (DMC), have important applications in the "green" chemical industry as raw materials and reagents for carbonylation and methylation reactions, replacing toxic phosgene and dimethyl sulfate, respectively [15–17]. DMC is the precursor for the manufacture of such engineering polymers as bis-phenol-A polycarbonates [18]. There have also been several patents disclosing their application as an octane booster [19,20]. The conventional manufacturing processes (oxidative carbonylation and phosgenation of methanol) [15–17] are highly hazardous (because both CO and $COCl_2$ are toxic). Eco-friendly routes for the synthesis of DMC include (1) synthesis from methanol and CO_2 [21–23]; (2) reaction of epoxides, CO_2, and methanol [24–26]; and (3) transesterification of cyclic carbonates with methanol [18,27–29]. The DMC yield is comparatively higher in the third option, which is in commercial use at the Chemei-Asahi Corporation (Taiwan) for the manufacture of bis-phenol-A polycarbonate [18]. Solid catalysts, such as ion-exchange resins, K-TS-1, Mg or

* Corresponding authors. Fax: +91 020 2590 2633.
E-mail addresses: d.srinivas@ncl.res.in (D. Srinivas), p.ratnasamy@ncl.res.in (P. Ratnasamy).

0021-9517/$ – see front matter © 2006 Published by Elsevier Inc.
doi:10.1016/j.jcat.2006.04.002

Ni-smectites, basic oxides (MgO/CaO and CaO/carbon), and hydrotalcites, have been known to catalyze the transesterification reaction [30–36]; however, the yield and selectivity of DMC are very low (<60%) over all of these solid catalysts. We have found that the double-metal cyanide Fe^{2+}–Zn^{2+} catalysts are more active/selective than the solid catalysts reported so far, and that they can be recycled several times with only negligible loss of activity.

2. Experimental

2.1. Catalyst preparation

In a typical preparation of Fe–Zn-1 catalyst, 0.01 mol of potassium ferrocyanide ($K_4[Fe(CN)_6]$; Merck, India) was dissolved in 40 mL of double-distilled water to prepare solution 1. In a separate beaker, solution 2 was prepared by dissolving 0.1 mol of $ZnCl_2$ (Merck, India) in 100 mL of distilled water and 20 mL of *tert*-butanol. A 15-g sample of tri-block copolymer, poly(ethylene glycol)-block-poly(propylene glycol)-block-poly(ethylene glycol) ($EO_{20}PO_{70}EO_{20}$; average molecular weight, 5800; Aldrich) was dissolved in a third beaker containing 2 mL of distilled water and 40 mL of *tert*-butanol to prepare solution 3. Solution 2 was added to solution 1 slowly over 1 h at 323 K under vigorous stirring. A white solid was precipitated. Solution 3 was then added to the above reaction mixture over 5–10 min, and stirring was continued for another 1 h. The solid thus formed was filtered, washed thoroughly with distilled water (500 mL) to remove all of the uncomplexed ions, and dried at 298 K for several hours. The material was activated at 453 K for 4 h (Fe–Zn-1). *Tert*-butanol acts as a complexing agent; tri-block copolymer, $EO_{20}PO_{70}EO_{20}$, acts as a co-complexing agent [5].

The effect of complexing and co-complexing agents on catalyst composition and reactivity was investigated by preparing two additional solid catalysts, Fe–Zn-2 and Fe–Zn-3, in a similar manner as described above, in the absence of co-complexing agent and in the absence of both complexing and co-complexing agents, respectively. Fe–Zn-2 was prepared without using the co-complexing agent $EO_{20}PO_{70}EO_{20}$ in the synthesis. Fe–Zn-3 was prepared in the absence of both the complexing and co-complexing agents.

2.2. Catalyst characterization

The metal and chloride ion content in the catalyst was estimated using a Rigaku 3070 E wavelength-dispersive X-ray fluorescence (XRF) spectrometer with Rh target energized at 50 kV and 40 mA. Elemental analyses (C, H, and N) were done on a Carlo-Erba 1106 analyzer. XRD patterns of the powdered samples were recorded on an Philips X'Pert Pro diffractometer using Cu-K_α radiation and a proportional counter detector. The surface area (S_{BET}) was determined by N_2 adsorption measurements at 77 K (NOVA 1200 Quanta Chrome equipment). Before N_2 adsorption, the samples were evacuated at 373 K. Diffuse-reflectance UV–visible spectra of the catalysts were recorded on a Shimadzu UV-2500 PC spectrophotometer using spectral-grade $BaSO_4$ as the reference material. IR spectra of the samples (as KBr pellets) were recorded on a Shimadzu 8201 PC FTIR spectrophotometer in 400–4000 cm^{-1} region. EPR measurements were obtained with a Bruker EMX spectrometer at X-band frequency ($\nu \approx 9.45$ GHz) and 80 K. Magnetic studies were done at 298 K using a Lewis coil force magnetometer (Series 300, George Associates, Berkeley, CA). X-ray photoelectron spectroscopy (XPS) measurements were conducted on a VG Microtech Multilab ESCA 3000 spectrometer with Mg-Kα radiation ($h\nu = 1253.6$ eV). Temperature-programmed desorption (TPD) measurements were performed using a Micromeritics AutoChem 2910 instrument. Thermal analysis was done on a Seiko DTA-TG 320 instrument under air (50 cm^3/min), at a ramp rate of 10 K/min, in the temperature range of 308–1090 K.

The acidity of the samples was studied by in situ FTIR spectroscopy and NH_3-TPD techniques. In pyridine adsorption measurements, about 5 mg of powdered catalyst was activated at 473 K, kept at that temperature for 3 h under nitrogen flush, and then cooled to 323 K. Then 20 μL of pyridine (in a nitrogen stream) was adsorbed onto the sample for 30 min. The temperature was raised slowly to a desired value and held at that temperature for another 30 min. The spectrum was then recorded (spectral range, 700–4000 cm^{-1}; resolution, 4 cm^{-1}; number of scans, 100). Difference spectra were obtained by subtracting the spectra of the sample before the adsorption of pyridine from the spectra of the pyridine-adsorbed sample.

For NH_3-TPD measurements, about 148 mg of the sample was activated at 473 K under He (30 mL/min). The sample was then cooled to 323 K and NH_3 (in He, 10:90 v/v; 45 mL/min) was adsorbed for 30 min. Desorption of NH_3 was followed at 323–473 K by increasing the temperature at a ramp rate of 10 K/min.

2.3. Reaction procedure: Transesterification of propene carbonate with alcohols

In the reaction procedure, 10 mmol of propene carbonate (PC), an excess of alcohol (2–10 equivalents), and a known amount of the solid double-metal cyanide catalyst (50–300 mg, activated at 453 K for 4 h) were placed in a Teflon-lined steel autoclave (100 mg). The autoclave was placed in a rotating hydrothermal reactor (Hero Co., Japan; rotating speed, 50 rpm), and the reactions were conducted at a specified temperature (373–443 K) for a specified period (2–8 h). After the reaction, the autoclave was cooled to 298 K, and the products were analyzed by gas chromatography (Varian 3800; CP-8907 column; 15 m × 0.25 mm × 0.25 μm). The products were identified by GC-MS (Shimadzu QP-5000; 30 m long, 0.25 mm i.d., with a 0.25-μm-thick capillary column, DB-1), GC-IR (Perkin Elmer 2000; BP-1 column; 25 m long, and 0.32 mm i.d.), and ^{1}H-NMR (Bruker AC 200). The products were also isolated in pure form by column chromatography (100–200 mesh silica gel) with CH_2Cl_2 as an eluent; the polarity of the eluent was increased with methanol. Transesterification of dimethyl carbonate was conducted in a similar manner.

The ^{1}H FT-NMR (δ values in ppm) of the isolated dialkyl carbonate products are as follows: DMC, 3.74 (singlet); diethyl carbonate (DEC), 1.27 (triplet), 4.15 (quartet); dipropyl carbonate, 1.25 (triplet), 1.80 (sextet), 3.89 (triplet); dibutyl carbonate, 1.31 (triplet), 1.82 (sextet), 1.93 (sextet), 4.02 (triplet); and dihexyl carbonate, 1.7, 2.2 (broad signal), 2.31 (multiplet), 4.45 (triplet).

3. Results and discussion

3.1. Catalyst characterization

3.1.1. Chemical composition

The compositions of Fe, Zn, and Cl ions in the double-metal cyanide Fe–Zn complexes (Fe–Zn-1, Fe–Zn-2, and Fe–Zn-3) estimated by XRF and carbon, hydrogen, and nitrogen (C, H and N) estimated by elemental analyses are presented in Table 1. Potassium ions are absent in the solid samples. Based on these average chemical compositions (XRF and elemental analyses) and X-ray structural information available on some known ferrocyanide complexes [6], a tentative structure is proposed for the Fe–Zn-1 complex (Scheme 1). Spectroscopic characterization studies described in subsequent sections provide additional support for the postulated structure. Attempts to grow single crystals of suitable quality for accurate single-crystal X-ray structural analysis have not been successful to date.

3.1.2. XRD

Fig. 1 shows X-ray diffractograms of powdered Fe–Zn complexes and their precursor compounds, $K_4Fe(CN)_6$ and $ZnCl_2$. The sharp peaks and typical XRD pattern for Fe–Zn catalysts, respectively, reveal that the catalysts are highly crystalline and contain negligible quantities of the starting compounds, $K_4Fe(CN)_6$ and $ZnCl_2$. Peak indexing [37] has revealed that the catalyst, Fe–Zn-1, crystallizes in a cubic lattice, with an unit cell parameter of 0.904 nm. XRD patterns of Fe–Zn-2 and Fe–Zn-3 (Fig. 1) are similar to that of Fe–Zn-1, except that the crystallinity of the former two is higher. Marginal shifts in peak position to lower 2θ values for the Fe–Zn-2 and Fe–Zn-3 catalysts are probably due to differences in the number of coordinated water and *tert*-butanol molecules (Table 1). The XRD pattern of the Fe–Zn-1 catalyst is characterized by the following peaks: 2θ (*hkl*)—16.92° (111), 20.16° (200), 22.33° (210), 24.77° (211), and 29.10° (221).

3.1.3. FTIR spectroscopy

IR spectroscopy is an ideal technique for differentiating the various coordination modes of cyanide groups in metal complexes. Except for the peaks due to coordinated water molecules, $ZnCl_2$ showed no additional IR bands in the spectral region of 4000–400 cm^{-1}. $K_4Fe(CN)_6$ showed an intense characteristic band at 2039 cm^{-1} due to ν(C≡N), which shifted to 2096 cm^{-1} for the Fe–Zn catalysts (Fig. 2). The free cyanide ion showed this band at 2080 cm^{-1} [38]. Previous studies [5–11] noted a similar shift in the position of this band to higher

Table 1
Catalyst composition and molecular formula

Catalyst	Preparation conditions	Fe:Zn:Cl molar ratio (XRF)[a]	Elemental analysis (%)[b]			Thermal analysis temperature range, K (%weight loss)			S_{BET} (m^2/g)	NH_3 desorbed (TPD) (mmol/g)	Possible molecular formula[c]
			C	H	N	Stage I	Stage II	Stage III			
Fe–Zn-1	Prepared using *t*-BuOH and $EO_{20}PO_{70}EO_{20}$	3.7:6.2:0.29	23.3 (22.5)	2.2 (2.6)	17.3 (18.7)	308–574 (21.6)	574–692 (16)	692–1090 (7.3)	51	1.96	$[Zn_3Fe_2(CN)_{10}(H_2O)_5(tert\text{-}BuOH)]\cdot 0.1ZnCl_2$
Fe–Zn-2	Prepared using *t*-BuOH but in the absence of $EO_{20}PO_{70}EO_{20}$	3.7:6.2:0.27	16.7 (17.4)	1.2 (1.5)	18.5 (20.8)	308–554 (15.6)	554–697 (15.7)	697–1090 (10)	43	1.87	$[Zn_3Fe_2(CN)_{10}(H_2O)_5]\cdot 0.1ZnCl_2$
Fe–Zn-3	Prepared in the absence of both *t*-BuOH and $EO_{20}PO_{70}EO_{20}$	3.7:6.2:0.27	18.0 (17.8)	1.4 (1.7)	18.9 (20.3)	308–612 (18.7)	612–684 (15.9)	684–1090 (7.0)	38	1.77	$[Zn_3Fe_2(CN)_{10}(H_2O)_6]\cdot 0.1ZnCl_2$

[a] The theoretical XRF values for all the catalysts are Fe:Zn = 4:6.
[b] Values in parentheses are the theoretical values.
[c] Proposed based on XRF and elemental analyses.

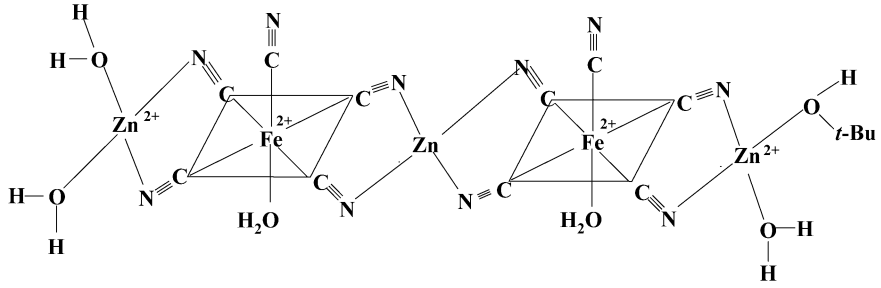

Scheme 1. Tentative structure of double metal cyanide Fe–Zn complex.

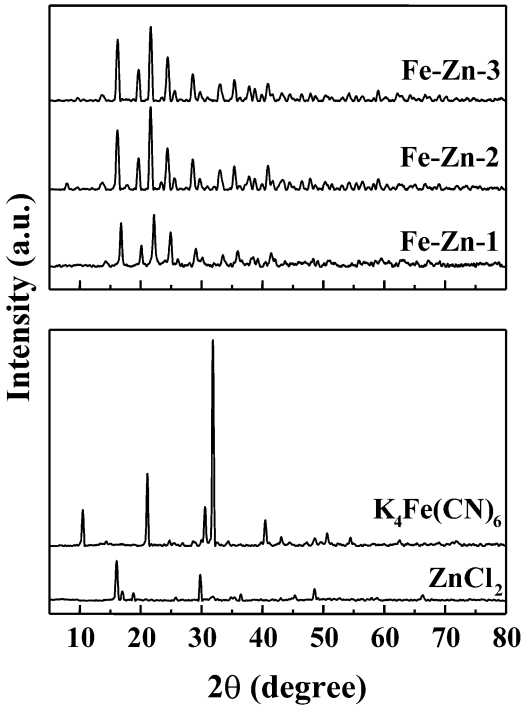

Fig. 1. XRD profiles of Fe–Zn double metal cyanide catalysts and the precursor compounds $ZnCl_2$ and $K_4Fe(CN)_6$. Fe–Zn-1, catalyst prepared in the presence of both *tert*-butanol and tri-block co-polymer. Fe–Zn-2, catalyst prepared in the presence of *tert*-butanol (tri-block co-polymer is absent). Fe–Zn-3, catalyst prepared in the absence of both *tert*-butanol and tri-block co-polymer.

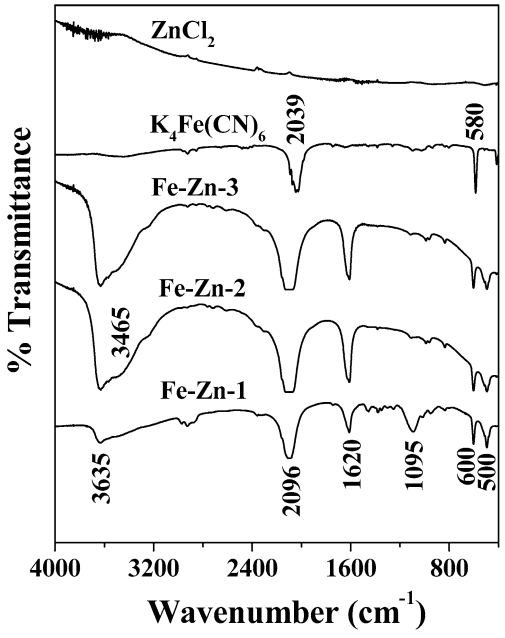

Fig. 2. IR spectra of $ZnCl_2$ and $K_4Fe(CN)_6$, and Fe–Zn based double metal cyanide catalysts (Fe–Zn-1, Fe–Zn-2 and Fe–Zn-3).

frequencies in related double-metal cyanide catalysts; for example, Co–Zn double-metal cyanides exhibited a shift of this band to 2195.9 cm^{-1} from 2133.4 cm^{-1}, corresponding to the precursor compound, $K_3Co(CN)_6$ [5]. In the case of Fe^{3+}–Zn^{2+} catalyst, this band appeared at 2179.2 cm^{-1} [6]. Multimetal cyanides (Co^{3+}–Fe^{2+}–Zn^{2+}) absorb at 2101.1 cm^{-1} [6]. The ν(C≡N) values for the metal complexes are generally higher than those for free CN^-. The shift of this band from 2039 cm^{-1} [for $K_4Fe(CN)_6$] to 2096 cm^{-1} (for Fe–Zn catalysts) in the present study suggests the formation of a new mixed-metal complex of ferrocyanide moiety and Zn^{2+} ions via bridging cyanide ligands [4]. Cyanide ions act not only as σ-donors (by donating electrons to Fe), but also as π-donors (by chelating to Zn). Electron donation raises the ν(CN), because electrons are removed from the 5σ orbital, which is weakly antibonding. Consequently, the ν(C≡N) band shifts to higher frequencies; π-back-bonding tends to decrease the ν(CN), because the electrons enter into the anti-bonding $2p\pi^*$ orbital. In general, CN^- is a good σ-donor and a poor π-acceptor. Thus, ν(CN) for the complexes is generally higher than the values for free CN^-. IR spectra also suggest that the cyanide ligands are oriented linearly between the divalent Zn and Fe, with the C atom possibly coordinated to Fe. The analogous cyano-bridged complex $[CpFe(PPh_3)(\mu\text{-}CN)_2ZnI(CH_3CN)]_2$ shows characteristic ν(CN) bands at 2092 and 2082 cm^{-1} [4], suggesting that in the complexes of the present study, cyanide bridging exists between the Fe^{2+} and Zn^{2+} moieties. All three Fe–Zn catalysts (Fe–Zn-1, Fe–Zn-2, and Fe–Zn-3) showed ν(CN) bands at identical positions, indicating that the method of preparation did not influence the primary structure of the Fe-$(CN)_n$-Zn moiety. The additional bands (Fig. 2) at 3635, 3465, 1620, 1095, 600, and 500 cm^{-1} and weak bands in the 1100–800 cm^{-1} region confirm the presence of water molecules and coordinated *tert*-butanol (1095 cm^{-1}) in Fe–Zn-1. Absence of the band at 1095 cm^{-1} (as well as any band in the 2800–3000 cm^{-1} region) in the spectra of Fe–Zn-2 and Fe–Zn-3 (Fig. 2) confirms the absence of *tert*-butanol in their structures.

3.1.4. DRUV–visible spectroscopy

$ZnCl_2$ showed no UV–visible bands in the 200–800 nm region. $K_4Fe(CN)_6$ showed an intense band at 236 nm and two medium-intensity bands at 278 and 330 nm (Fig. 3). Whereas the latter two bands are attributed to ligand-to-metal (Fe) charge transfer (LMCT) transitions, the former (at 236 nm) is attributed to π–π^* charge transfers in the CN ligand [39]. In the case of Fe–Zn catalysts, the LMCT bands shifted to the higher energy side (266 and 315 nm, respectively), probably due to donation of antibonding electrons to both Fe^{2+} and Zn^{2+} ions. This shift in position of the LMCT bands lends additional support to the conclusion derived from the FTIR results, namely that the Fe–Zn catalysts contain bridging cyano groups between Fe and Zn. No additional absorption bands were observed for both $K_4Fe(CN)_6$ and the double-metal cyanide Fe–Zn catalysts in the visible region, indicating that Fe, in the latter, is in a low-spin +2 oxidation state corresponding to $^1A_{1g}$ ground state. The electronic transition from $^1A_{1g}$ to excited triplet states is Laporte-forbidden, and hence no d–d transitions were observed in the visible region. When the catalyst was activated at higher temperatures (ca. >573 K), a resolved band was observed in the visible region at 496 nm, indicating a change in the structure and oxidation state of Fe from +2 to +3 at higher temperatures.

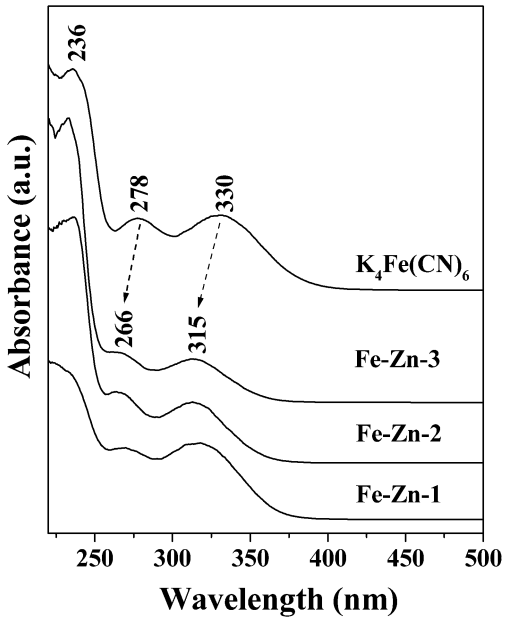

Fig. 3. Diffuse reflectance UV–visible spectra of $K_4Fe(CN)_6$ and Fe–Zn based double metal cyanide catalysts (Fe–Zn-1, Fe–Zn-2 and Fe–Zn-3).

3.1.5. EPR spectroscopy and magnetic measurements

The oxidation states of the catalyst materials were confirmed by subjecting them to magnetic susceptibility and EPR spectral measurements. All of the Fe–Zn catalysts of the present study are diamagnetic at 298 K. The compounds are EPR-silent, indicating that Fe is in a low-spin, +2, oxidation state.

3.1.6. X-Ray photoelectron spectroscopy

X-Ray photoelectron spectra of Fe–Zn-1 catalyst activated at 473 and 673 K are shown in Fig. 4. The binding energy of the zinc atom shifted to a lower value in Fe–Zn-1 (1021.4 eV) compared with $ZnCl_2$ (1023.7 eV) [2,6]. Similarly, at 473 K, the binding energy of $Fe(2p_{3/2})$ shifted to a lower value in Fe–Zn-1 (707 eV) compared with $K_4Fe(CN)_6$ (708 eV). These shifts in the binding energies of Zn and Fe to lower values are indicative of changes in the electronic environment of both Zn and Fe on complexation and formation of double-metal cyanide Fe–Zn catalysts. On calcination at 673 K, the binding energy of Fe in Fe–Zn complexes changed to 711 eV. The N(1s) binding energies in the samples activated at 473 and 673 K were 397 and 399 eV, respectively. This peak, for $K_4Fe(CN)_6$, was observed

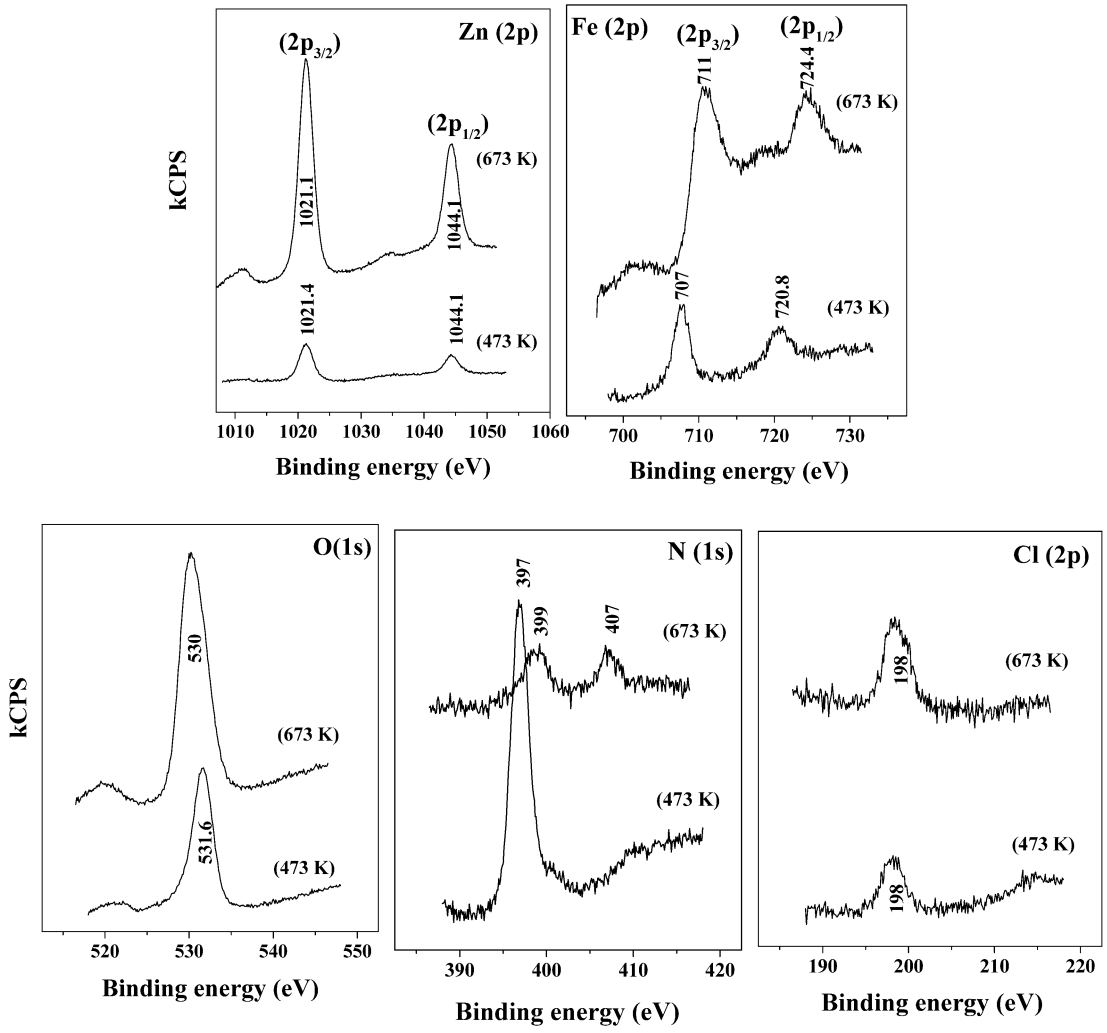

Fig. 4. XPS of Fe–Zn double metal cyanide catalyst (Fe–Zn-1) activated at 473 and 673 K.

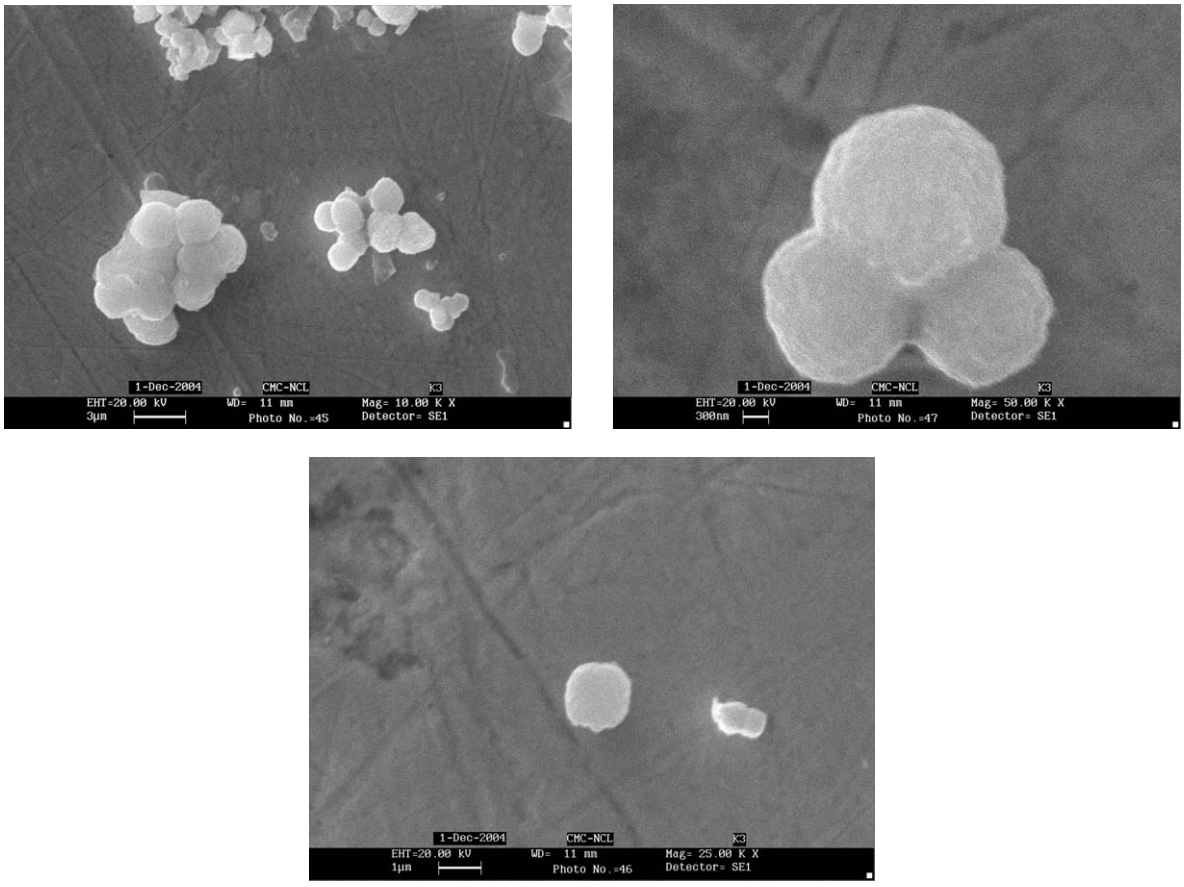

Fig. 5. Scanning electron micrographs of Fe–Zn-1 catalyst.

at 398 eV. A very weak peak arising from Cl(2p) (probably from $ZnCl_2$ residual impurity) appeared at 198 eV.

3.1.7. Scanning electron microscopy

The catalyst material (Fe–Zn-1) is highly crystalline and has a spherical morphology (Fig. 5). The particle size of the catalyst is in the range of 1–3 µm.

3.1.8. Acidic properties

3.1.8.1. DRIFT spectroscopy of adsorbed pyridine Fig. 6 depicts the difference IR spectra (DRIFT mode) of adsorbed pyridine on the double-metal cyanide Fe–Zn catalysts. The absence of peaks at 1639 and 1546 cm^{-1} in the difference IR spectra (Fig. 6) indicates the absence of Brönsted acid sites; the peaks at 1608 and 1450 cm^{-1} in Fe–Zn-1 indicate the presence of strong Lewis acid sites [40,41]. Fe–Zn-2 and Fe–Zn-3 showed a similar spectral pattern. But the intensities of the IR bands were lower than those of Fe–Zn-1, indicating a lower density of the acid sites in the catalysts prepared without using *tert*-butanol or copolymer. As expected, the intensity of the IR peaks decreased with increasing temperature.

3.1.8.2. NH_3-TPD The acidity of the samples was also estimated independently by NH_3-TPD. After activation at 473 K, NH_3 was adsorbed at 323 K, and its desorption was monitored at 323–473 K. The Fe–Zn catalysts showed a broad, asymmetric desorption feature that could be deconvoluted into three desorption peaks with maxima at 357, 382, and 417 K (Fig. 7). The desorption feature at 357 K can be attributed to physisorbed NH_3; the features at 382 K and 417 K are assigned to desorption from weak and strong Lewis acid sites, respectively. The total amount of NH_3 desorbed from the Fe–Zn-1, Fe–Zn-2, and Fe–Zn-3 samples was 1.96, 1.87, and 1.77 mmol/g, respectively. The amount of NH_3 desorbed from the 417 K peak (strong Lewis acid site) was 0.57 mmol/g for Fe–Zn-1 and 0.29 mmol/g for Fe–Zn-2. NH_3 desorption from the 382 K peak (weak Lewis acid site) was 0.85 mmol/g for Fe–Zn-1 and 0.83 mmol/g for Fe–Zn-2. Thus, Fe–Zn-1 contains a larger number of Lewis acid sites. Although more detailed investigations are still needed, we propose that the terminal Zn^{2+} ions in the Fe–Zn structure (Scheme 1) adsorb pyridine and NH_3 and function as Lewis acid sites. Fe in the catalyst structure acts as a metal-dispersing agent and a stabilizer of the cyano-bridged complex.

3.1.9. Thermal stability

Thermal stability of the double-metal cyanide Fe–Zn catalysts were investigated by XRD, diffuse reflectance UV–visible, FTIR, EPR, and thermogravimetric analyses. On calcination in air for 4 h, Fe–Zn-1 retained its characteristic crystalline structure up to 473 K; beyond that, the complex decomposed and new crystalline phases formed that were identified as $ZnFe_2O_4$ [2θ values (*hkl*): 18.33° (111), 30.08° (220), 35.45° (311), 36.43° (222), 43.27° (400), 53.53° (422), 56.71° (511), 62.32°

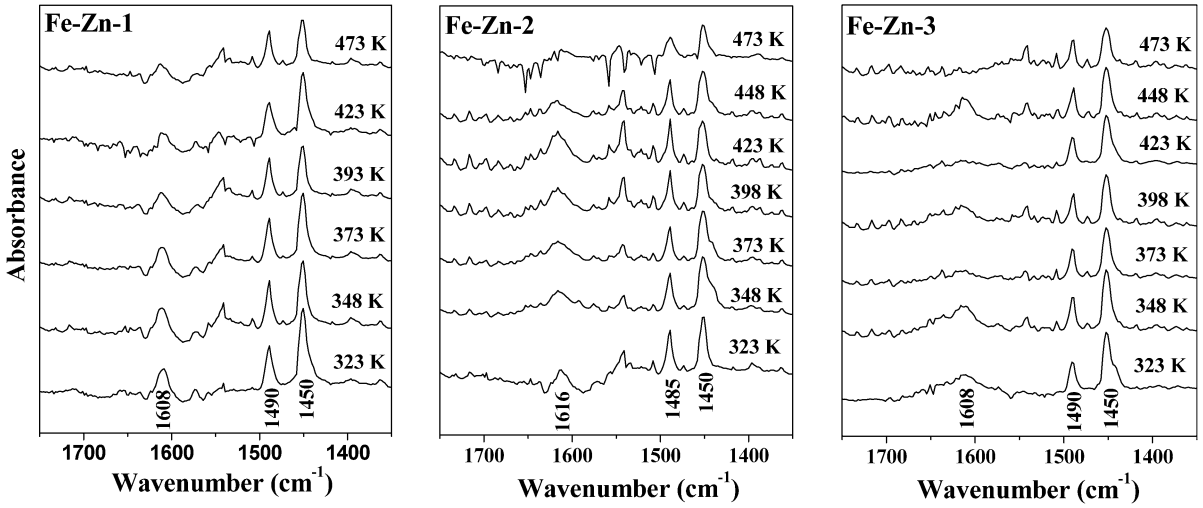

Fig. 6. DRIFT spectra of adsorbed pyridine on Fe–Zn double metal cyanide catalysts.

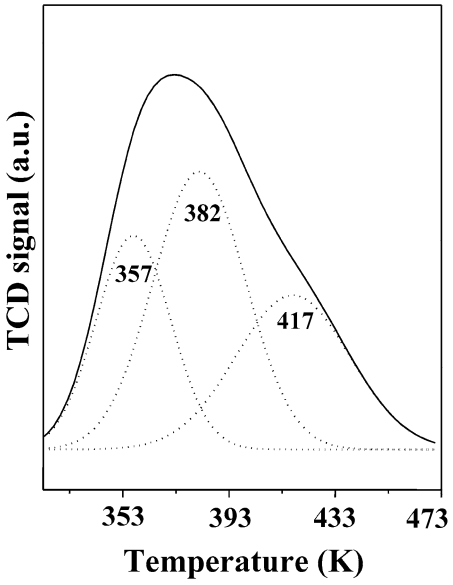

Fig. 7. NH_3-TPD over Fe–Zn-1 catalyst.

(440); JCPDS#77-0011] and ZnO [2θ values (hkl): 32.03° (100), 34.47° (002), 36.43° (101), 48.16° (102), 56.71° (110) 63.03° (103), 66.73° (200), 68.18° (112), 69.42° (201), 71.13° (004); JCPDS#79-2205] (Fig. 8).

Even if some crystalline iron oxide phases remained in the calcined samples, their concentrations were significantly smaller than those of $ZnFe_2O_4$ and ZnO. The characteristic LMCT bands (266 and 315 nm) and the π–π^* transition peaks (236 nm) of the catalyst sample in the UV–visible spectrum vanished above 473 K, consistent with the decomposition of the cyanide group at elevated temperatures (Fig. 8(b)). The characteristic band of CN^- at 2096 cm^{-1} in the IR spectrum [Fig. 8(c)] disappeared above 573 K, and new peaks, probably due to nitrate-like species, appeared at 1495 and 1380 cm^{-1}. Recall that depletion of nitrogen, significant changes in binding energy, and marked surface enrichment of Zn, Fe, and O were observed by XPS in samples activated above 473 K (Fig. 4). The shift in binding energy of Fe($2p_{3/2}$) from 707 to 711 eV indicates a change in the oxidation state of iron from +2 to +3 and formation of $ZnFe_2O_4$-type species [42]. In addition, sam-

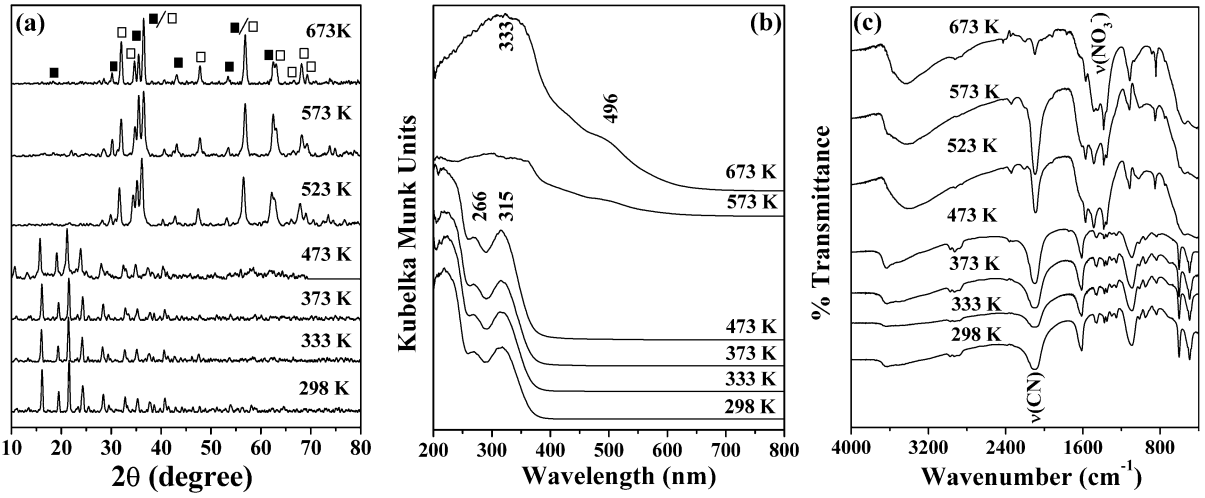

Fig. 8. Thermal stability of Fe–Zn-1: (a) XRD, (b) diffuse reflectance UV–visible, and (c) FTIR. XRD peaks corresponding to $ZnFe_2O_4$ (■) and ZnO (□) are indicated.

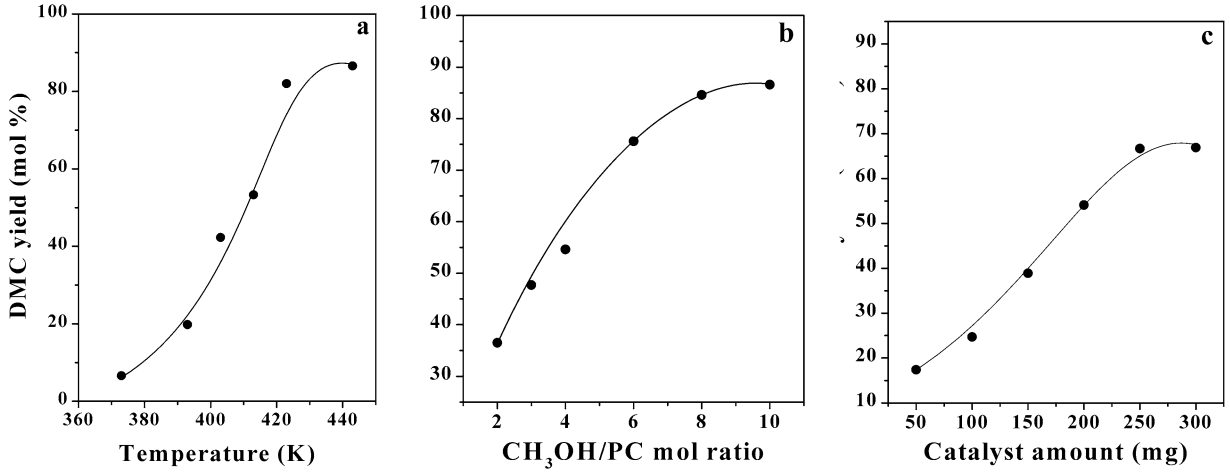

Fig. 9. Transesterification of propene carbonate (PC) with methanol. Influence of (a) reaction temperature, (b) CH_3OH to PC ratio and (c) amount of catalyst on DMC yield. Reaction conditions for (a): catalyst Fe–Zn-1 (activated at 453 K for 4 h), 0.25 g; PC, 10 mmol; methanol, 100 mmol, reaction time, 8 h. Reaction conditions for (b): catalyst Fe–Zn-1 (activated at 453 K for 4 h), 0.25 g; reaction temperature, 443 K; PC, 10 mmol; reaction time, 8 h. Reaction conditions for (c): PC, 10 mmol; methanol, 100 mmol; reaction temperature, 443 K; reaction time, 4 h.

ples that initially were EPR-silent became active when activated above 473 K and showed characteristic signals at $g \approx 2.34$ and 2.005, typical of high-spin Fe^{3+} ions [43]. The shift in the peak corresponding to N(1s) in XPS from 397 to 399 eV on calcination in air above 473 K is further evidence of the decompositon of cyanide (probably to nitrates) [43]. The specific surface area (S_{BET}) of calcined Fe–Zn-1 decreased as follows: 51.6 m^2/g at 298 K, 47.2 m^2/g at 333 K, 41.6 m^2/g at 473 K, and 19 m^2/g at 673 K. Thus, all of the structural and spectral techniques used indicate that the Fe–Zn catalyst is stable up to about 498 K, and beyond that the cyanide groups decompose, forming crystalline ZnO and $ZnFe_2O_4$ phases.

Thermal analysis (see Table 1) showed three stages of weight loss: stage I (at 308–573 K), stage II (at 573–690 K), and stage III (at 873–1090 K). Stage I corresponds to the desorption of the water and *tert*-butanol molecules; state II is due to decomposition of the cyanide group, followed by transformation of the double-metal cyanide complexes into metal nitrates and carbonates; and stage III is attributed to the complete decomposition of the material into the metal oxides $ZnFe_2O_4$ and ZnO.

3.2. Catalytic activity

Transesterification of propene carbonate (PC) with different alcohols yielded equimolar amounts of the corresponding dialkyl carbonate and 1,2-propylene glycol. The reaction occurred only in the presence of the catalysts and did not proceed over $ZnCl_2$ or $K_4Fe(CN)_6$. The double-metal cyanide complexes prepared using $K_3Fe(CN)_6$ (wherein the iron is in the ferric state) instead of $K_4Fe(CN)_6$ were less active. The influence of temperature, methanol/propene carbonate ratio, and catalyst amount on the yield of DMC in the transesterification of PC with methanol is shown in Fig. 9. The yields reported are the isolated yields. DMC was isolated from the reaction mixture by column chromatography. The yield of DMC increased with increasing temperature. A maximum DMC yield of 86% was obtained at 443 K. As expected, the DMC yield increased with increasing methanol concentration [Fig. 9(b)]. Transesterification is an equilibrium reaction; for complete transesterification of one mole of PC, stoichiometrically two moles of alcohol are needed. An excess amount of alcohol drives the reaction toward the transesterified product. Various dialkyl carbonates could be synthesized by transesterification of propene carbonate with different alcohols over Fe–Zn-1 catalyst (Table 2). The yield of dialkyl carbonate decreased with increasing alkyl chain length. At the end of the reaction, the solid catalyst was filtered, washed, with methanol and acetone, air-dried at room temperature, and recycled. No significant loss in activity

Table 2
Transesterification of propene carbonate with various alcohols over double metal cyanide Fe–Zn catalyst (Fe–Zn-1)[a]

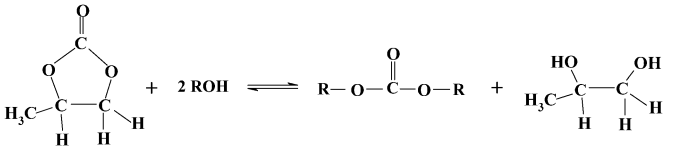

Run no.	ROH	Dialkyl carbonate yield (mol%)[b]	TON[c]
1	Methanol	86.6	26
2	Methanol (**recycle-1**)	83.2	25
3	Methanol (**recycle-2**)	83.5	25
4	Methanol (**recycle-3**)	84.9	25
5	Methanol (**recycle-4**)	83.2	25
6	Methanol (**recycle-5**)	82.6	25
7	Ethanol	79.4	24
8	Propanol	77.5	23
9	Butanol	69.3	21
10	Hexanol	62.5	19
11	Benzyl alcohol	77.8	23

[a] Reaction conditions: Fe–Zn-1 (preactivated at 453 K for 4 h), 0.25 g; PC, 10 mmol; ROH, 100 mmol; reaction temperature, 443 K; reaction time, 8 h.
[b] Product isolated by column chromatography. Isolated yield is reported. 1,2-propene glycol was formed in an equivalent amount.
[c] TON = moles of PC converted per mole of catalyst.

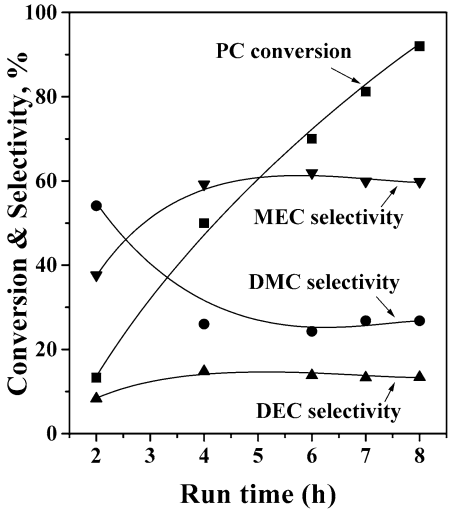

Fig. 10. Transesterification of propene carbonate with an equimolar mixture of ethanol and methanol. Reaction conditions: Fe–Zn-1 (activated at 453 K for 4 h), 0.25 g; PC, 10 mmol; alcohol mixture (methanol–ethanol), 100 mmol; methanol:ethanol (molar ratio), 1; temperature, 443 K.

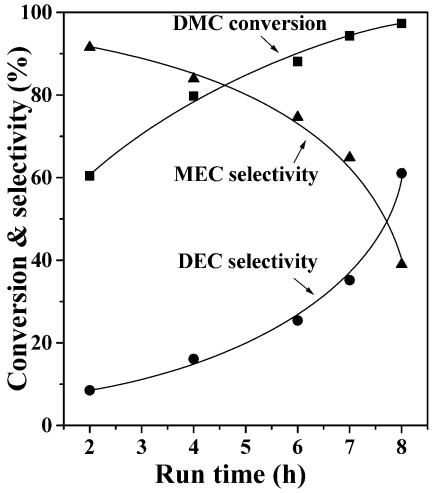

Fig. 11. Transesterification of dimethyl carbonate (DMC) with ethanol producing methyl ethyl carbonate (MEC) and diethyl carbonate (DEC). Reaction conditions: Fe–Zn-1 (activated at 453 K for 4 h), 0.25 g; DMC, 10 mmol; ethanol, 100 mmol; temperature, 443 K.

Table 3
Reaction of dimethyl carbonate with various alcohols over Fe–Zn-1 catalyst[a]

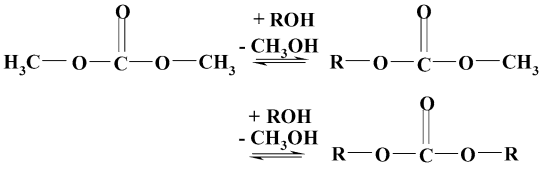

Catalyst activation temperature (K)	ROH	DMC conversion (mol%)	Product selectivity (%)		TON
			Methyl alkyl carbonate	Dialkyl carbonate	
473	Ethanol	97.4	39.1	60.9	29
473	Propanol	93.4	65.1	34.9	28
473	Butanol	94.6	69.8	30.2	28
473	Hexanol	92.8	73.9	26.1	28
473	Benzyl alcohol	96.0	36.6	63.4	29
523	Ethanol	54.0	19.5	80.5	–
573	Ethanol	47.6	18.5	81.5	–
673	Ethanol	37.8	20.0	80.0	–

[a] Reaction conditions: Fe–Zn-1, 0.25 g; DMC, 10 mmol; ROH, 100 mmol; reaction temperature, 443 K; reaction time, 8 h.

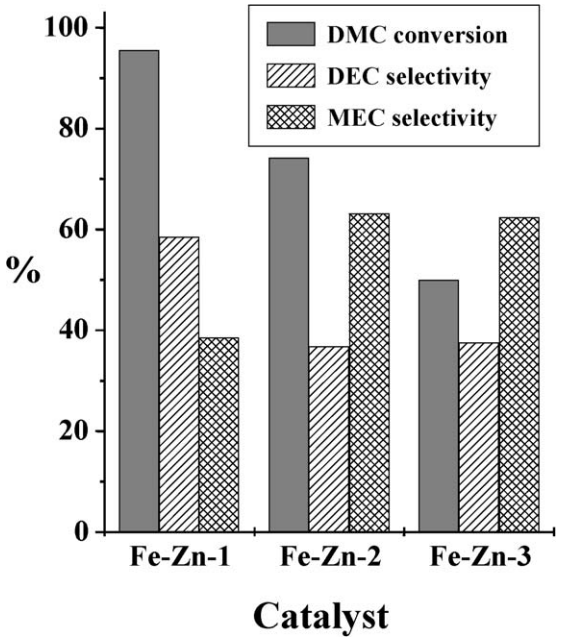

Fig. 12. Transesterification of DMC with ethanol over different Fe–Zn catalysts. Reaction conditions: catalyst (activated at 453 K for 4 h), 0.25 g; DMC, 10 mmol; ethanol, 100 mmol; temperature, 443 K; reaction time, 8 h.

was observed in at least five recycling experiments (Table 2). In the transesterification of PC with an equimolar mixture of methanol and ethanol (Fig. 10), DMC was the initial, main product. Beyond 2 h, the concentration of methyl ethyl carbonate (MEC) increased significantly at the expense of DMC. After 8 h, the products contained a mixture of DMC, MEC, and DEC.

Conversions were higher in the transesterification of DMC (Table 3; Fig. 11). In the transesterification of DMC with ethanol, the catalytic activity decreased in the following order: Fe–Zn-1 > Fe–Zn-2 > Fe–Zn-3 (Fig. 12). This order parallels the variation in their surface area and relative acidity (Table 1). The novel catalysts of the present study are significantly more active than those reported earlier, including ion-exchange resins, K-TS-1, Mg/Ni-smectites, basic oxides (MgO/CaO and CaO/carbon), and hydrotalcites [30–36]. They are also reusable, with negligible loss in activity. The mechanism of double-metal cyanide-catalyzed ring-opening polymerization of propene oxide has been reported previously [6]; a similar reaction pathway is also expected here. The terminal Zn atoms are the active sites, which assist in the cleavage of the cyclic carbonate ring. This is followed by transesterification with the alcohols/alcoholates present in the reaction medium. A tentative reaction mechanism over Lewis acid Zn^{2+} cations in the Fe–Zn double-metal cyanide catalyst is shown in Fig. 13. The pK_a of the alcohol and substituents (e.g., methyl in the case

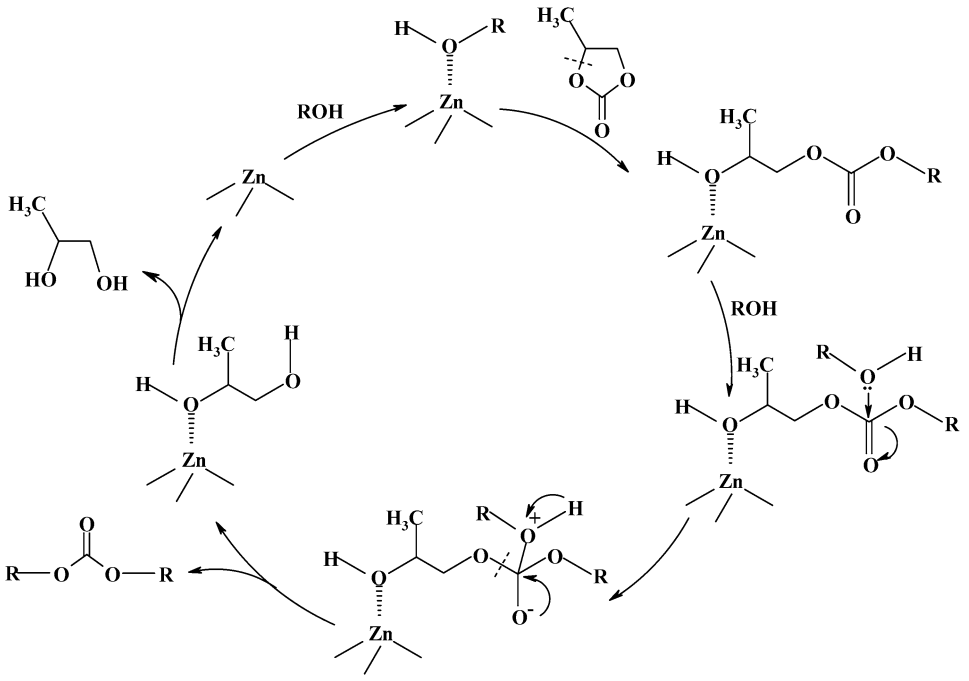

Fig. 13. Tentative reaction mechanism for transesterification of propene carbonate with alcohols (ROH) over Lewis acid Zn^{2+} cations in Fe–Zn double metal cyanide catalysts.

of PC) and the pK_a of the alcohol influence the cleavage of the cyclic carbonates and also determine the rate of the reaction.

On calcining the catalysts above 473 K, the conversion of DMC decreased drastically to levels observed for other solid catalysts (30–40%) [30–36]; however, the selectivity values remained high (Table 3). The loss in catalytic activity on calcination is due to the formation of iron and zinc oxide phases noted earlier (Fig. 8). A more detailed study of the catalytic properties of this mixed oxide phase will be published later.

4. Conclusion

The catalytic activity of solid Fe–Zn double-metal cyanide complexes for the transesterification of carbonates has been evaluated. These catalysts are more active than the other solid catalysts hitherto reported for this reaction. DMC, for example, was synthesized with 100% selectivity and an isolated yield of >86% over these catalysts. Various dialkyl carbonates could be synthesized by transesterification of PC with different alcohols. Unsymmetrical carbonates were synthesized by the reaction of PC with a mixture of alcohols (methanol–ethanol, for example). The Fe–Zn catalysts are reusable, with little loss in activity. The accessible and Lewis-acidic Zn^{2+} cations are the possible active sites in transesterification reaction.

Acknowledgments

R.S. thanks the Council of Scientific and Industrial Research (CSIR), New Delhi, for a Senior Research Fellowship. This work was done as part of the network project “Catalysis and Catalysts” (P23-CMM005.3) sponsored by CSIR.

References

[1] I. Kim, M.J. Yi, S.H. Byun, D.W. Park, B.U. Kim, C.S. Ha, Macromol. Symp. 224 (2005) 181.
[2] M.J. Yi, S.-H. Byun, C.-S. Ha, D.-W. Park, I. Kim, Solid State Ionics 172 (2004) 139.
[3] (a) S. Chen, Z. Hua, Z. Fang, G. Qi , Polymer 45 (2004) 6519;
(b) S. Chen, G.-R. Qi, Z.-J. Hua, H.-Q. Yan, J. Polym. Sci. A: Polym. Chem. 42 (2004) 6519.
[4] D.J. Darensbourg, M.J. Adams, C. Yarbrough, Inorg. Chem. 40 (2001) 6543.
[5] I. Kim, J.-T. Ahn, S.-H. Lee, C.-S. Ha, D.-W. Park, Catal. Today 93–95 (2004) 511.
[6] I. Kim, J.-T. Ahn, C.-S. Ha, C.-S. Yang, I. Park, Polymer 44 (2003) 3417.
[7] M.O. James, L.L. Donald, L.G. Robin, US Patent 6,359,101 (2002).
[8] K.G. McDaniel, M.J. Perry, J.E. Hayes, WO 9,914,258 (1999).
[9] H. van der Hulst, G.A. Pogany, J. Kuyper, US Patent 4, 477, 589 (1984).
[10] J. Milgrom, US Patent 3, 404, 109 (1968).
[11] R.J. Herold, US Patent 3, 278,459 (1966).
[12] S. Chen, N. Xu, J. Shi, Prog. Org. Coat. 49 (2004) 125.
[13] S. Chen, L. Chen, Colloid Polym. Sci. 282 (2004) 1033.
[14] S. Chen, L. Chen, Colloid Polym. Sci. 281 (2003) 288.
[15] P. Tundo, M. Selva, Acc. Chem. Res. 35 (2002) 706.
[16] D. Delledonne, F. Rivetti, U. Romano, App. Catal. A: Gen. 221 (2001) 241.
[17] M.A. Pacheco, C.L. Marshall, Energy Fuels 11 (1997) 2.
[18] S. Fukuoka, M. Kawamura, K. Komiya, M. Tojo, H. Hachiya, K. Hasegawa, M. Aminaka, H. Okamoto, I. Fukawa, S. Konno, Green Chem. 5 (2003) 497.
[19] P.J. Jessup, S.G. Brass, M.C. Croudace, US Patent 4,600,408 (1986).
[20] D.M. Dillon, R.Y. Iwamoto, US Patent 4,891,049 (1990).
[21] J.-C. Choi, L.-N. He, H. Yasuda, T. Sakakura, Green Chem. 4 (2002) 230.
[22] K. Tomishige, Y. Ikeda, T. Sakaihori, K. Fujimoto, J. Catal. 192 (2000) 355.
[23] S.-i. Fujita, B.M. Bhanage, Y. Ikushima, M. Arai, Green Chem. 3 (2001) 87.
[24] B.M. Bhanage, S.-i. Fujita, Y. Ikushima, M. Arai, Appl. Catal. A: Gen. 219 (2001) 259.

[25] Y. Chang, T.J. Han, Z. Liu, W. Wu, L. Gao, J. Li, H. Gao, G. Zhao, J. Huang, Appl. Catal. A: Gen. 263 (2004) 179.
[26] Y. Li, X-q. Zhao, Y.-j. Wang, Appl. Catal. A: Gen. 279 (2005) 205.
[27] J. De, P. Johannes, J.-P. Lange, US Patent 6,835,858 (2004).
[28] M. Tojo, F. Shinsuke, K. Mamoru, US Patent 5,847,189 (1998).
[29] M. Tojo, K. Oonishi, US Patent 6,479,689 (2002).
[30] T. Tatsumi, Y. Watanabe, K.A. Koyano, Chem. Commun. (1996) 2281.
[31] D. Srinivas, R. Srivastava, P. Ratnasamy, Catal. Today 93 (2004) 127.
[32] R. Srivastava, D. Srinivas, P. Ratnasamy, Stud. Surf. Sci. Catal. 154C (2004) 2703.
[33] T. Wei, M. Wang, W. Wei, Y. Sun, B. Zhong, Green Chem. 5 (2003) 343.
[34] T. Wei, M. Wang, W. Wei, Y. Sun, B. Zhong, in: D.G. Morrell (Ed.), Catalysis of Organic Reactions, Marcel Decker, New York, 2003, p. 659, chap. 58.
[35] Y. Watanabe, T. Tatsumi, Microporous Mesoporous Mater. 22 (1998) 399.
[36] B.M. Bhanage, S.-i. Fujita, Y. He, Y. Ikushima, M. Shirai, K. Torii, M. Arai, Catal. Lett. 83 (2002) 137.
[37] S. Chen, P. Zhang, L. Chen, Prog. Org. Coat. 50 (2004) 269.
[38] K. Nakamoto, Infrared and Raman Spectra of Inorganic and Coordination Compounds, third ed., Wiley, New York, 1978, p. 266.
[39] A.B.P. Lever, Inorganic Electronic Spectroscopy, second ed., Elsevier, Amsterdam, 1984.
[40] B. Chakraborty, B. Viswanathan, Catal. Today 49 (1999) 253.
[41] M. Hunger, U. Schenk, M. Breuninger, R. Gläser, J. Weitkamp, Microporous Mesoporous Mater. 27 (1999) 261.
[42] C.D. Wagner, W.M. Riggs, L.E. Davis, J.F. Moulder, G.E. Muilenberg (Eds.), Handbook of X-Ray Photoelectron Spectroscopy, Perkin-Elmer Co., Eden Prairie, MN, 1979.
[43] J.R. Wertz, J.E. Bolton, Electron Spin Resonance: Elementary Theory and Practical Applications, McGraw–Hill, New York, 1972.